CLASP stabilizes microtubule plus ends after severing to facilitate light-induced microtubule reorientation

Authors

Jelmer J. Lindeboom[1,2*], Masayoshi Nakamura[1,3*], Marco Saltini[4], Anneke Hibbel[2], Ankit Walia[1,5], Tijs Ketelaar[2], Anne Mie C. Emons[2,4], John C. Sedbrook[6], Viktor Kirik[6], Bela M. Mulder[2,4] and David W. Ehrhardt[1,7].

* Equal contribution.

Author affiliations

1 Department of Plant Biology, Carnegie Institution for Science, Stanford, CA 94305, USA.
2 Laboratory of Cell Biology, Wageningen University, 6708 PB Wageningen, Netherlands.
3 Institute of Transformative Bio-Molecules (WPI-ITbM), Nagoya University, Nagoya 464-8601 Japan.
4 Institute AMOLF, 1098 XG Amsterdam, Netherlands.
5 Sainsbury Laboratory, University of Cambridge, Cambridge CB2 1LR, UK.
6 School of Biological Sciences, Illinois State University, Normal, IL 61790, USA.
7 Department of Biology, Stanford University, Stanford, CA 94305, USA

Corresponding author:

David W. Ehrhardt

ehrhardt@stanford.edu

Introduction

Eukaryotic cells build microtubule arrays with specific and diverse architectures to perform essential cellular functions, including division and morphogenesis. Central to building and reorganizing cytoskeletal arrays is the creation of new polymers. While nucleation has been the major focus of study for microtubule creation, it has been proposed that severing might also be used to create new populations of microtubules[1]. This generative capacity of severing was recently demonstrated directly in higher plants, where it was shown that severing by katanin drives the reorientation of cortical microtubule arrays by amplifying a new population of polymers as part of the phototrophic response[2]. An important and unanswered question about how severing can lead to the creation of new microtubule arrays is how the freshly severed ends are stabilized such that severing does not lead instead to array dissolution. Here we identify the conserved protein CLASP as a potent *in vivo* stabilizer of new plus ends generated by katanin mediated severing in *Arabidopsis*. This activity was required for rapid cortical array reorientation in response to light signaling. CLASP was found to increase the fraction of plus ends rescued after severing by approximately 4.3-fold, an increase shown by computational modeling to likely be a key factor for amplifying new populations of microtubules created by severing to reorganize cortical microtubule arrays.

Results

Microtubule reorientation in plus tip mutants

In the cortical arrays of higher plants, new microtubule plus ends can be created either by microtubule nucleation[3,4] or microtubule severing[2,5,6]. When new microtubules arrays are built by nucleation, the growing ends assembled at nucleation complexes are stabilized by the GTP state of newly added tubulin dimers[7] and by proteins that associate with growing ends[8], some of which are recruited by the GTP cap[8]. However, new plus ends generated by severing are likely created behind the GTP-cap. These new plus ends shrink immediately when created *in vitro*[9,10]. By contrast, when severing creates new plus ends in vivo, they frequently initiate new growth without observable shrinkage[2]. The factors that act *in vivo* to stabilize new plus ends created by severing to permit this generation of microtubules have not been identified. Several microtubule plus-end-tracking proteins (+TIPs) have been found in the model plant *Arabidopsis*, some conserved across phyla and others plant-specific. We asked if one or more of these +TIPs might act as a specific plus end rescue factor after severing to support creation of a new cortical array by a severing-driven mechanism.

To investigate plus end stabilization following severing in a functional and physiological context, we utilized the rapid reorientation of cortical microtubule arrays in higher plants as driven by blue light perception. Interphase cells in higher plants feature cortical microtubule arrays where microtubules are associated with the plasma membrane. In rapidly elongating cells, cortical

microtubules are highly ordered and oriented transversely to the main axis of cell growth. As part of the phototrophic response, perception of blue light by phototropin photoreceptors in epidermal cells of the plant axis drives a rapid reorientation of these arrays by 90° to a longitudinal orientation. This occurs by upregulation of katanin mediated severing where cortical microtubules intersect, or crossover, with a preference for severing of the newer of the two microtubules[2,11]. Growth of the plus ends created by severing builds and amplifies a new population of microtubules at 90° to the existing array. A functional consequence of this reorientation is redirection of the trajectories of cellulose synthase complexes as they build the cell wall, thus remodeling cell wall structure.

We tested mutants in three families of +TIP proteins for their ability to support rapid cortical array reorientation. Encoded by three genes in *Arabidopsis*, *EB1a-c*, all three EB1 loci are disrupted in the triple mutant *3x-eb1*[12]. Cytoplasmic-linker-associated protein (CLASP) is conserved across both plants and animals. It is represented by a single gene in *Arabidopsis*, where loss of function (*clasp*) results in significant loss of cell growth anisotropy[13,14]. SPIRAL1 (SPR1) is specific to algae and plants[15]. In *Arabidopsis*, SPR1 is part of a six-gene family where loss of SPR1 function itself (*spr1*) causes pronounced chiral twisting of plant organs and loss of cell growth anisotropy. Time lapsed imaging of microtubule dynamics was accomplished by introducing the tubulin marker 35S-YFP-TUA5 into the *spr1*, *clasp* and *3x-eb1* mutants (Fig. 1a and Video 1), and quantitation of local microtubule orientation over time was performed with the ImageJ plugin LOCO[2] (Fig. 1b and c). We found that both the *3x-eb1* and *clasp* mutants had a higher degree of transverse order than WT before the start of blue light excitation ($P < 0.05$ Mann-Whitney U test compared to WT) (Fig. 1d). Importantly, when the speed with which the longitudinal order was built up over time was measured, we observed that *3x-eb1* and *clasp* mutants were in addition significantly slower than WT ($P < 0.05$ Mann-Whitney U test compared to WT) (Fig. 1e). By contrast, although *spr1* mutants have pronounced morphogenetic phenotypes, no significant effect was measured in either initial array order nor reorientation speed. Thus, both the *3x-eb1* and *clasp* mutant start off with a higher degree of transverse order while at the same time showing a slower generation of longitudinal microtubule order, with both effects additively resulting in slower light-stimulated microtubule reorientation.

The reorientation defects we found for the *3x-eb1* and *clasp* mutants may be due to specific effects on plus end rescue after severing, to changes in basic microtubule dynamics, or possibly severing itself. To assess these possibilities, we first measured individual microtubule dynamics at the onset of reorientation then explored the consequences of measured changes in microtubules behaviors with modeling and computer simulation studies.

Microtubule dynamics in plus tip mutants

To measure basic microtubule dynamics, we generated kymographs from the reorientation movies (Fig. 2a) and traced the trajectories of microtubule ends (see Methods). We observed

quantitatively small yet statistically significant differences in growth velocities between WT and all the tested +TIP mutants ($P < 0.001$ Mann-Whitney U test compared to WT for all genotypes) (Fig. 2b, Table S1). *spr1* and *clasp* showed higher growth velocities than WT, while plus ends in *3x-eb1* grew more slowly than WT. We found that *spr1* mutants had a slower shrinkage velocity than WT ($P < 0.05$ Mann-Whitney U test), while *3x-eb1* and *clasp* mutants both had a higher shrinkage velocity than WT (Fig. 2c, $P < 0.05$ and $P < 0.01$, respectively, Mann-Whitney U test). When making transitions between shrinking to growth, we observed that the *clasp* mutants had a significant rescue defect compared to WT (Fig. 2d, $P < 0.05$ rate ratio exact test). No significant differences were measured in catastrophe rates between WT and any of the +TIP mutants (Fig. 2e). In summary, we found small but significant differences in microtubule dynamics between WT and *spr1*, *3x- eb1* and *clasp,* the most notable being the rescue defect in *clasp*. The possible significance of these small but significant differences to the amplification of new microtubule array will be explored below in computer modeling studies.

Severing in plus tip mutants

To assess the function of +TIPs in stabilizing microtubule ends after severing, we analyzed the outcomes of microtubule crossover formation in WT and *spr1*, *3x-eb1* and *clasp* mutant backgrounds expressing YFP-TUA5 as a microtubule marker. For each crossover, we marked the location, time of creation, time of resolution, whether the crossover was resolved by severing or by depolymerization of either crossover partner, and whether the old microtubule (the preexisting microtubule) or the new microtubule (the microtubule that crosses the preexisting one to form the crossover) at the crossover got severed (See Methods). We also scored if the newly created plus end was shrinking or growing (Fig. 3a and Video 2, Fig. 3b and Video 3, respectively).

We observed no significant difference (Fisher's exact test) between the likelihood of observing severing after crossover formation in WT and *3x-eb1,* both showing a 44% probability of severing (Fig. 3c). For the *spr1* mutant we measured a 42% probability of severing per crossover, which is significantly lower than in WT ($P < 0.05$ Fisher's exact test). Interestingly, the *clasp* mutant showed a 52% probability of severing per crossover, which is significantly higher than WT ($P < 0.05$ Fisher's exact test) (Fig. 3c).

The severing likelihood depends both on the kinetics of severing itself (e.g. katanin recruitment, activation and action), and on microtubule dynamics, as crossovers get resolved either by microtubule severing or depolymerization beyond the crossover location. To better assess severing activity itself we measured the time from crossover formation to the time that optical evidence of severing was observed, a quantity we term the sever waiting time (Fig. 3d and Fig. S1). When crossovers are resolved by microtubule dynamics, a sever waiting time is of course not calculated. When comparing the observed sever waiting time distributions we found that both *spr1* ($P < 0.01$ Mann-Whitney U test) and *3x-eb1* ($P < 0.001$ Mann-Whitney U test) have a significantly longer mean

sever waiting time compared to WT. Strikingly, the *clasp* mutant shows a significant reduction in sever waiting time for microtubule severing than we found for WT ($P < 0.001$ Mann-Whitney U test). In summary, microtubule severing activity is increased in the *clasp* mutant, suggesting that CLASP antagonizes severing activity.

Rescue after severing in +TIP mutants

During blue light-induced microtubule reorientation, most of the new growing microtubules are created by katanin mediated severing[2], but an outstanding question was how the new plus ends get stabilized right after severing, as the new plus end that is created by severing most likely lacks the stabilizing GTP cap. We therefore compared the fates of the new plus end that was created by severing in WT and the plus tip mutants (Fig. 3e). In WT, we found that the new microtubule was observed in a growing state 14% of the time immediately after severing, which was not significantly different from the 12% we found in the *3x-eb1* mutant background (Fisher's exact test). The rescue probability after severing was significantly reduced to 9% ($P < 0.05$ Fisher's exact test) in the *spr1* mutant. Most strikingly, in the *clasp* mutant, we only observed the new plus end created by severing in a growing state in 3% of the time ($P < 0.05$ Fisher's exact test), which is a ~4.3-fold reduction compared to WT, showing that CLASP plays an important role in stabilizing microtubule plus ends after severing.

Rescue is associated with CLASP localization but not crossovers

In higher plants, GFP-tagged CLASP protein accumulates along the lattice of cortical microtubules well behind the tip[13,14] in distinct punctae[14], in addition to dynamic plus ends[14]. We confirmed this punctate localization pattern along the lattice in the etiolated hypocotyl cells used in this study (Fig. 4a, Video 4) and also observed that labeled CLASP accumulates in areas of high microtubule curvature (Fig. 4b, Video 5). Such distributed prepositioning to along the lattice might be useful for rescue function when new ends are generated mid-lattice by severing. In support of this possibility, *in vitro* studies had shown that *Schizosaccharomyces pombe* CLASP also labeled microtubules heterogeneously along their length, and that locations of high CLASP concentration were correlated with rescue[16]. To ask if rescue *in vitro* is associated with local CLASP concentration, we analyzed the ratio of CLASP to microtubule signal and related this to the behavior of shrinking microtubule ends (Fig. 4c, see Methods). We quantified the CLASP to MT signal ratio in 2716 frames where the microtubule continued shrinking and 301 instances where the microtubule got rescued. When we compared the signal intensity ratio between shrinking and rescue frames we indeed found a significantly higher CLASP to microtubule ratio at locations where rescue was observed ($P < 0.001$ Mann-Whitney U test, one-tailed) (Fig. 4d), indicating that CLASP is indeed a rescue factor for interphase microtubules in plants.

A recent study reported an increased rescue rate at microtubule crossovers in animal cells[17]. To test if rescues at crossovers are also more likely in *Arabidopsis* we used kymograph analysis to compare the microtubule intensity measured at shrinking plus ends and at locations where plus ends were rescued. Microtubule signal intensity is higher at crossovers due to the combined signal of microtubules at crossover sites. If there is indeed an increased microtubule rescue at crossovers in plant, we would predict a positive correlation between microtubule signal and microtubule rescue for shrinking microtubules. However, we found that the relative microtubule signal intensity is not significantly higher for plus ends that are being rescued (N = 301) compared to those that continue shrinking (N = 2716) in *Arabidopsis* ($P > 0.98$ Mann-Whitney U test, one-tailed) (Fig. S3). In addition, analysis of the ratio of GFP-CLASP to microtubule signals during crossover formation indicated that CLASP was actually under-represented at crossovers rather than over represented (Figure 5c, N = 839 crossovers in 6 plants, note standard error bars for CLASP/MT signal before and after crossover). Taken together, these data indicate that sites of CLASP concentration along the microtubule lattice appear to be functional as sites of increased rescue likelihood *in vivo*, which may help explain the special function of CLASP in plus end rescue follow severing. However, CLASP does not accumulate specifically at crossovers, nor are crossovers themselves hot spots for rescue in plant interphase arrays.

Simulations for microtubule propagation efficiency by severing in plus tip mutants

Our measurements of microtubule array reorientation revealed that CLASP is a key player in cortical array remodeling in response to light stimulation. Measurements of microtubule behaviors revealed two differences that stood out when comparing *clasp* mutants to WT and the other +TIP mutants: reduction of the intrinsic rescue rate from 1.56 to 1.12 events/minute, and decrease of the probability of plus end rescue after severing from 15% to 3%. Significant but quantitatively more modest changes in other parameters of polymer dynamics, such as growth and shrinkage rates, were also observed. To better assess the contributions and significance of these changes in polymer behaviors and dynamics in amplifying a new population of microtubules that drives the reorientation, we designed and employed a probabilistic model for generating longitudinal microtubules by severing and rescue. The simulations were parameterized with estimates from our *in vivo* measurements of microtubule dynamics and crossover outcomes in WT, *spr1*, *3xeb1* and *clasp* backgrounds (See Table S1), together with measurements of the spacing between transverse microtubules (Fig. S2 a-d and Methods). In a single simulation run, a single microtubule was initiated transversely to a grid of pre-existing microtubules and its fate and those of its progeny were assessed as a function of time. For each genotype or experimental test, $N = 5 \times 10^4$ runs were performed to build up a probabilistic picture of microtubule fate. The results were analyzed in terms of two measures: the probability that a microtubule, and all of its progeny created at severing events, die out (extinction probability), and the

expected number of surviving descendants of a microtubule at a fixed time point after initiation (Fig. 5a and b).

For all genotypes, simulations resulted in net microtubule amplification (Fig. 5b) despite a finite probability of failure for each trial (Fig. 5a). This outcome is consistent with experimental observations, where some degree of reorientation was observed for all genotypes, even in the most severe mutant, *clasp*. These results can be understood by examination of the values for the basic microtubules dynamics (growth and shrinkage speeds, transition frequencies), which for all genotypes are in the so-called unbounded growth regime, a state where the measured polymer dynamics predict net polymer growth over time, rather than a state of equilibrium. The measure for this effect is the average growth velocity[18]. A positive average growth velocity itself leads to net amplification because individual microtubules are expected to survive on average in spite of being severed[19].

While all simulations showed a degree of amplification, the magnitudes of amplification and the probabilities of extinction varied markedly by genotype and mirrored the measured defects on reorientation speed, with *clasp* being the most defective in both amplification and having the highest likelihood of extinction, followed by *3x-eb1* and *spr1* (Fig. 5a and b). Thus, not only do the measured microtubule dynamics and behaviors in *clasp* predict the lowest rate of net amplification, but also the highest likelihood of amplification failure.

In order to understand which of the two major changes in microtubule dynamics observed in the *clasp* mutant might more greatly affect the speed of amplification, the reduction in the intrinsic rescue rate (r_c), or the quantitatively larger reduction in the rescue rate after severing ($P_{s,+}$), we created two synthetic *in silico* mutants: WT with the *clasp* mutant rescue rate (WT/*clasp*-r_c), and WT with the *clasp* rescue rate after severing (WT/*clasp*-$P_{s,+}$). As shown in Fig. 5c, both mutations have a similarly detrimental effect on extinction probability with respect to WT. However, amplification in WT/*clasp*-$P_{s,+}$ is slower than that in WT/*clasp*-r_c, indicating that the change in $P_{s,+}$ dominates the amplification defect in *clasp* (Fig. 5d). Further, the reduction in $P_{s,+}$ by itself almost completely reproduces the *clasp* phenotype. Taken together, the simulation analyses quantify the importance of CLASP function in the amplification process of the number of new longitudinal microtubules, and support the hypothesis that the dominant function of CLASP in building a new a new array by severing-driven microtubule amplification is by its specific function in rescue after severing.

Discussion

In the cortical arrays of higher plants, new growing microtubule plus ends are created both by microtubule nucleation[3,4] and by microtubule severing[2,5,6]. A recent *in vitro* study has shown that templated nucleation, whether from nucleation complexes or microtubules seeds, is an energetically unfavorable process that can be made more efficient by microtubule associated proteins[20]. The lack of a stabilizing GTP-cap presents a second energetic challenge to the creation of new microtubules from

severed ends. Our data identify CLASP as a potent factor for promoting growth from plus ends created by severing ends *in vivo*. This function might therefore be due to lowering the energetic barrier of templated polymer initiation from these ends, by antagonizing the transition to catastrophic disassembly in the absence of a GTP-cap, or perhaps both.

The precise mechanisms by which CLASP might act to stabilize severed ends and promote regrowth have not been identified. Observation of free tubulin at sites of CLASP accumulation in vitro suggested the hypothesis that CLASP might act to concentrate tubulin locally to promote rescue[16]. An alternative, and not mutually exclusive, possibility is that interaction of CLASP with the microtubule lattice provides stabilizing energy. Proteins that influence microtubule stability often do so based on preferential binding to αβ-tubulin of specific curvature (reviewed by Brouhard and Rice, 2014)[21]. Here we indeed find stronger relative CLASP fluorescence for highly curved microtubule regions (Fig. 5b and Video 5). Therefore, an alternative model for CLASP's action as a rescue factor is that CLASP could halt the progression of curvature that occurs in microtubule protofilaments during depolymerization by binding to tubulin. It is interesting to note that we found that CLASP function antagonizes microtubule severing at microtubule crossovers (Fig. 3c and d). Since microtubule severing requires deformation of the microtubule lattice to break lateral protofilament bonds, it is possible that CLASP offers protection against severing by the same mechanism that stabilizes microtubule plus ends.

Severing is a fundamental tool employed by cells across phyla to manipulate and regulate cytoskeletal arrays. Here we report the function of CLASP in stabilizing the plus ends generated by severing to enable severing to rapidly build a new microtubule array. Severing is also proposed to build essential microtubule arrays in neurons, epithelial cells and meiocytes[1], but the proteins used to stabilize the ends generated by severing have not been identified in these cells. As CLASP is conserved across animals and plants, our studies suggest that it is CLASP is an excellent candidate to investigate.

Methods

Plant material

Microtubules were marked by introducing the 35S-YFP-TUA5 construct[22] into four genetic backgrounds of *Arabidopsis thaliana*, all ecotype Col-0. Wild type[22] and *spr1-6*[23] transformants were described previously. For this study 35S-YFP-TUA5[22] was introduced into *cls1-1*[14] by *Agrobacterium* mediated transformation. In the manuscript, *spr1-6* and *cls1-1* are referred to as *spr1* and *clasp*.

Introduction of 35S-YFP-TUA5 into a triple mutant *eb1* background was accomplished as follows. The *Ateb1a-2* T-DNA insertional mutant (WiscDsLox481-484J12; insertion in the 7th exon of AT3G47690) and the *Ateb1b-2* T-DNA insertional mutant (WiscDsLox331A08; insertion in the 6th intron of At5g62500; see Galva et al., 2014[12] for additional details) were obtained from the

Arabidopsis Knockout Facility (University of Wisconsin Biotechnology Center[24]). The *Ateb1c-2* T-DNA insertional mutant (SALK_018475; insertion in the 3rd exon of AT5G67270) was generated at the Salk Institute[25] and obtained from the Arabidopsis Biological Resource Center (ABRC). *Ateb1a-2*, *Ateb1b-2*, and *Ateb1c-2* mutant plants were cross-pollenated then progeny self-pollenated to generate the *Ateb1a-2 Ateb1b-2 Ateb1c-2* triple mutant. T-DNA insertions were tracked and homozygosity determined by performing PCR analysis using alkali-prepped seedling cotyledon extracts[26] as templates along with the primers/ primer pairs listed in Table S2. We refer to this triple eb1 knockout mutant line as *3x-eb1* throughout the manuscript. This *3x-eb1* line was then transformed with the same 35S-YFP-TUA5 microtubule marker[22].

For the MT and CLASP dual labelled line we transformed the *clasp1-1* expressing AtCLASP-YFP-AtCLASP[14] with a ProUBQ10-mCherry-TUA5 construct. This microtubule reporter was generated by amplifying a 634bp genomic upstream regulatory fragment of UBQ10 from pUBN-GFP-DEST[27]. The CaMV 35S promoter was excised from the modified pMDC43 vector encoding mCherry[14] and replaced by the UBQ10 fragment. LR recombinase (Invitrogen) was used to introduce the *Arabidopsis* TUA5 cDNA[28] into the modified pMDC43 Gateway binary vector to generate a ProUBQ10-mCherry-TUA5 construct. The binary vector harboring the construct was then introduced into WT Arabidopsis plants (Col-0) by Agrobacterium-mediated transformation using the floral dip method[29]. Transgenic T1 plants were selected for Hygromycin B selection. T2 progeny plants with normal growth and development (with the exception of mild twisting) were used to for experiments.

Plant growth

Seeds were surface sterilized with a 70% ethanol solution, stratified for 3 days at 4 °C, and sown on 1% agar containing Hoagland's No. 2 salts at pH 5.7. After 1 h of light exposure on the clean bench, the seedlings were grown in darkness for 60–72 h at 22 °C.

Specimen mounting

Seedlings were mounted under red safelight conditions to prevent de-etiolation[30]. Seedlings were placed gently on a cover slip in sterile water and affixed with a 1 mm thick 1% agarose pad. To reduce specimen drift, the mounted seedling was rested for 20-30 minutes before observation.

Microscopy

All observations were made in epidermal cells in the upper hypocotyl, a region where cell expansion is rapid in 3 day old etiolated seedlings. The time lapse imaging of the YFP-TUA5 labeled lines was performed at 5s time intervals for a duration of 30 minutes on a CSU-X1 spinning-disk confocal head mounted on a Leica DMI6000B microscope with Adaptive Focus Control (Leica) and a 100× Plan Apo 1.4 N.A. oil immersion objective described previously[2]. For each image, excitation was supplied by a 488 nm laser for 300 ms at 4.5 mW as measured at the end of optical fiber feeding

the spinning disk unit.

We performed imaging of cells dual labeled with YFP-CLASP and mCherry-TUA5 with a Yokogawa CSU-X1 spinning disk head mounted on a Nikon Eclipse Ti body using as described previously[28,31]. Exposures were acquired every 2.5s, using a 491nm laser to excite YFP-CLASP for 500 ms, and a 591nm laser to excite mCherry-TUA5 for 300 ms.

Reorientation analysis

We used the ImageJ plugin LOCO[2] to analyze microtubule reorientation after blue light induction. To assure that there was sufficient transverse order at the start of stimulation to measure the transition to longitudinal orientation, datasets were selected for analysis where the initial transverse order parameter was lower than 0.1. We used a MATLAB script to extract the microtubule orientation information from the LOCO output[2].

Analysis of microtubule dynamics

The growing and shrinking ends of individual labeled microtubules were visualized by time-phased subtraction of image time series acquired from seedlings expressing YFP-TUA5 as described previously[2]. Trajectories of segmented growing ends in selected regions of interest were created blindly using the PlusTipTracker software package[32]. These paths were then used to measure microtubule dynamic parameters using a custom pipeline in MATLAB. First, the paths created by PlusTipTracker were used generate kymographs. All kymographs generated were examined, and those showing clear evidence of plus ends growth at least 5 frames were then traced by hand using a custom graphical user interface in MATLAB. Finally, polymerization and depolymerization velocities, as well as the frequency rescue and severing rates, were calculated from the kymograph traces. This protocol allowed for less biased sampling and measurement of end dynamics than what might result from selection by eye.

Analysis of crossovers

To analyze the formation and resolution of microtubule crossovers in plants expressing YFP-TUA5 in the different genetic backgrounds, we marked for every observed crossover in the region of interest the x and y coordinates, start and end time of the crossover, angles of the old and new microtubules, and whether the old and/or new microtubule at the crossover got severed (Video 6). In the case of no severing, we marked whether the crossover disappeared because of depolymerization from the plus or minus end. If a severing event took place at the crossover we documented whether the new plus end created by severing was initially growing or shrinking.

This analysis of crossover formation and resolution was also performed on the image time series used for the analysis of CLASP and MT signal at crossovers. We first registered the image

using the microtubule channel using StackReg[33] followed by photobleaching correction using an exponential fit to total signal intensity of the original images series using ImageJ. We then isolated a 7-by-7-pixel region centered around each of the crossover coordinates. The 1 pixel wide outer border was used for determining the background signal intensity for both CLASP and MT signal. We discarded the highest 12 pixel values, as they typically represent the microtubule signal of the two microtubules forming the crossover. We took the median intensity value of the remaining pixels as the local background for the crossover for each individual frame of each crossover. To calculate the crossover signal intensity, we subtracted the background value calculated from the border from each of the pixels from the inner 5-by-5 pixels of the crossover ROI. After background subtraction, we summed the intensity values of the 5-by-5-pixel region to obtain the total crossover intensity. We then normalized the signal intensity by dividing the maximum ROI intensity for each individual crossover. The normalized crossover intensities were calculated for both the CLASP and MT signal, and the crossover event intensities were aligned with each other over time based on either the start or end frame of the crossover event. We calculated the CLASP to MT signal ratio by dividing the normalized CLASP intensity by the normalized MT intensity. The standard errors for this ratio estimate were calculated from the error propagation of the standard errors of the separate CLASP and MT signal intensities.

Quantification of microtubule and CLASP intensity at sites of rescue

For both the microtubule and CLASP channel, we first applied image registration and bleaching correction in ImageJ. For each frame, we normalized the intensity values per frame to the median intensity value after dividing the intensity values into 10 equal sized bins and discarding the values in the highest and lowest bin to remove outliers. We then used these movies to extract kymographs using the method described above in "Analysis of microtubule dynamics". We traced the edge of the microtubule signal in the kymograph by hand and used a MATLAB script to identify microtubule shrinkage and rescue evens. Since CLASP in *Arabidopsis* cells has been reported to be a plus end tracking protein[14], we wanted to exclude any bias of CLASP measurement that may occur due to rescue and subsequent recruitment of CLASP to the growing plus end. We therefore extracted the CLASP and microtubule intensity in a 3-pixel wide range over the two frames immediately before that location is reached by the depolymerizing microtubule end. We assessed the averaged and normalized pixel intensity of these ROIs and sorted them into two groups. One group in which the shrinking microtubule continues to shrink in the following frame, and the other group where the microtubule is rescued in the following frame.

Microtubule bundle distances

To calculate the distribution of distances in between transverse microtubules along the longitudinal axis of the cell, we rotated the first image in each acquired time series of cells expressing

YFP-TUA5 so that the long axis of the plant is on the vertical axis. We applied a rolling ball background subtraction with a radius of 30 pixels to each image in ImageJ and selected the vertical midline of the image. We used the MATLAB function findpeaks to extract all the peaks in the data and used the findpeaks output parameter peak prominence to identify locations of possible microtubule fluorescence intensity. We determined that for our data, peak prominence values above 0.015 were reliably associated with locations of microtubule signal while values below generally represent background signal. We then calculated the distances between detected microtubule signal peaks. Fig. S2 shows an example for WT with an overlay of the detected peaks in cyan on the fluorescence image used as input data. This measurement was performed for YFP-TUA5 expressed in WT, and in *spr1, 3x-eb1,* and *clasp* mutants.

Stochastic model

To better understand the importance of the stabilization of microtubule plus ends generated by severing, we set up a stochastic model of longitudinal microtubules undergoing dynamic instability in a grid of stable transverse microtubules. This choice of holding transverse microtubules is related to our interest in studying only the first stage of the process, in particular the first 500 s after the exposure to light. The distance d between neighboring transverse filaments is distributed according to the distribution,

$$f(d) = \begin{cases} 0, & \text{if } \ d \leq 0.5\mu m \\ \\ \frac{1}{D}\, e^{-\frac{d}{D}}, & \text{if } \ d > 0.5\mu m \end{cases}$$

where the length D is chosen such that the mean spacing between transverse microtubules d_{avg} is consistent with the distances experimentally measured between microtubules/bundles (Table S1, Fig. S2).

The model follows the evolution of a single longitudinal microtubule, modelled as a straight line, undergoing dynamic instability at its plus end in such a grid of transverse microtubules. The microtubule is nucleated with initial length zero and in the growing state. Dynamic parameters of the model are the growing speed v^+, the shrinking speed v^-, the catastrophe rate r_c (rate of passing from the growing to the shrinking state) and the rescue rates r_c (rate of passing from the shrinking to the growing state). To perform the simulations, we used the experimental measurements of the speeds and the transition rates as the values for our dynamic parameters (Fig. 2, Table S1).

When the plus end crosses a transverse microtubule, it creates a crossover. At every crossover, there is a competition between two different effects: either the crossover is erased by the shrinkage of the plus end due to dynamic instability, or it leads to a severing event. Whether one

effect wins against the other is determined by an intrinsic severing waiting time distribution $W_{k,\theta}(t)$, where $W_{k,\theta}(t)$ is the Gamma probability density function[34],

$$W_{k\theta}(t) = \frac{t^{k-1}}{\theta^k \Gamma(k)} e^{-\frac{t}{\theta}},$$

with k and θ as scale and shape parameters of the distribution, and $\Gamma(k)$ as the Euler gamma function[35]

$$\Gamma(k) = \int_0^{+\infty} dx\, x^{k-1} e^{-x},$$

Given the impossibility to measure the intrinsic waiting time distribution for the severing, due to the deletion of some crossovers because of dynamic instability, we have chosen k and θ such that the distribution of the severing waiting time conditional to the fact that the severing happened, optimally fits the experimentally measured one (see Fig. S4). Given our assumption that the effect of katanin is different for different mutants because of difference in microtubule dynamics and severing properties, the parameters of the distribution are different for WT, *3x-eb1*, *spr1* and *clasp* mutants. Since we are only interested in the behavior of longitudinal microtubules in the first 500 s of the process, we limit severing to only the longitudinal microtubules.

To properly model the behavior of newly-created plus ends after severing observed in the experiments, we introduce the probability $P_{s,+}$ as their probability of rescue after severing, i.e. as the probability that the newly-created plus end grows just after the severing event. Consequently, the probability that the newly-created plus end shrinks just after the severing event is $1-P_{s,+}$ (see Fig. 5).

Every simulation consists of one longitudinal microtubule nucleated in the grid of transverse microtubules, and it lasts for 500 simulated seconds. After that time, the output of the simulation can be either extinction, i.e. the initial microtubule and all its progeny have completely depolymerized due to dynamic instability, or amplification, i.e. there are one or more longitudinal microtubules still alive. We average our simulation results over 5 x 10^4 trials.

The main results of these simulation studies are reported in the main text. In order to better quantify the effect of $P_{s,+}$ and the effect of r_r on the speed of amplification, we performed a sensitivity analysis. In the first case, having WT parameters as background we tune $P_{s,+}$, from 0 to 0.25, and we count the number of longitudinal microtubules in the simulation after 500s. In the second case we repeat the same procedure, keeping the WT value for $P_{s,+}$ = 0.15, and tuning the intrinsic rescue rate r_r, from 0.76 events/min to 2.09 events/min. The reason for the choice of these two values for the intrinsic rescue rate is the following: given our interest in the behavior of microtubules in the

unbounded growth regime, the rate $r_r = 0.76$ event/min is the smallest rescue rate required to be in the unbounded growth regime, i.e. it is the value that allows the average growth speed[18]

$$J = \frac{v^+ r_r - v^- r_c}{r_r + r_c}.$$

to be non-negative, in particular to be $J = 0$. Taking WT values as our reference values, we can see that

$[P_{s,+} = 0.15] : [P_{s,+} = 0.25] = [r_r = (1.56\text{-}0.76)$ events/min$] : [r_r = (2.09\text{-}0.76)$ events/min],

motivating our choice to take 2.09 events/min as the intrinsic rescue rate. Fig. S5 shows that the effect on the amplification if we change $P_{s,+}$ is stronger than if we change r_r, supporting our hypothesis that the key parameter for the speed of amplification is the fraction of rescue after severing.

Acknowledgements

We thank Zdeněk Lánský for advice on image analysis, David Quint and Luke Rice for helpful discussion. This work was supported by the Carnegie Institution for Science (DWE); NSF grant 1158372 (DWE), and the Human Frontier Science Program (MN). The work of MS is supported by the European Research Council Synergy grant MODELCELL. The work of BMM is part of the research programme of the Netherlands Organisation for Scientific Research (NWO).

Author contributions

DWE, JJL, MN, VK, TK and AMCE designed experimental strategy. JJL, MN and AH carried out experiments. JJL, MN and DWE analyzed data. BM and MS designed and performed the simulations. JJL, DWE, MN, BM and MS wrote the manuscript. AW and JS provided biological materials. All authors contributed to editing the manuscript.

Competing interests

The authors declare that they have no competing financial interest.

References

1. Roll-Mecak, A. & Vale, R. D. Making more microtubules by severing: a common theme of noncentrosomal microtubule arrays? *The Journal of Cell Biology* **175,** 849–851 (2006).
2. Lindeboom, J. J. *et al.* A mechanism for reorientation of cortical microtubule arrays driven by microtubule severing. **342,** 1245533–1245533 (2013).
3. Wasteneys, G. O. & Williamson, R. E. Reassembly of microtubules in Nitella tasmanica: assembly of cortical microtubules in branching clusters and its relevance to steady-state microtubule assembly. *Journal of Cell Science* **93,** 705–714 (1989).
4. Nakamura, M., Ehrhardt, D. W. & Hashimoto, T. Microtubule and katanin-dependent dynamics of microtubule nucleation complexes in the acentrosomal Arabidopsis cortical array. *Nat. Cell Biol.* **12,** 1064–1070 (2010).
5. Wightman, R. & Turner, S. R. Severing at sites of microtubule crossover contributes to microtubule alignment in cortical arrays. *The Plant journal* **52,** 742–751 (2007).
6. Zhang, Q., Fishel, E., Bertroche, T. & Dixit, R. Microtubule severing at crossover sites by katanin generates ordered cortical microtubule arrays in Arabidopsis. *Curr Biol* **23,** 2191–2195 (2013).
7. Mitchison, T. & Kirschner, M. Dynamic instability of microtubule growth. *Nature* **312,** 237–242 (1984).
8. Akhmanova, A. & Steinmetz, M. O. Control of microtubule organization and dynamics: two ends in the limelight. *Nat. Rev. Mol. Cell Biol.* **16,** 711–726 (2015).
9. Walker, R. A., Inoué, S. & Salmon, E. D. Asymmetric behavior of severed microtubule ends after ultraviolet-microbeam irradiation of individual microtubules in vitro. *The Journal of Cell Biology* **108,** 931–937 (1989).
10. Tran, P. T., Walker, R. A. & Salmon, E. D. A metastable intermediate state of microtubule dynamic instability that differs significantly between plus and minus ends. *The Journal of Cell Biology* **138,** 105–117 (1997).
11. Zhang, Q., Fishel, E., Bertroche, T. & Dixit, R. Microtubule severing at crossover sites by katanin generates ordered cortical microtubule arrays in Arabidopsis. *Curr Biol* **23,** 2191–2195 (2013).
12. Galva, C. *et al.* The microtubule plus-end tracking proteins SPR1 and EB1b interact to maintain polar cell elongation and directional organ growth in Arabidopsis. *Plant Cell* **26,** 4409–4425 (2014).
13. Ambrose, J. C., Shoji, T., Kotzer, A. M., Pighin, J. A. & Wasteneys, G. O. The Arabidopsis CLASP gene encodes a microtubule-associated protein involved in cell expansion and division. *Plant Cell* **19,** 2763–2775 (2007).
14. Kirik, V. *et al.* CLASP localizes in two discrete patterns on cortical microtubules and is required for cell morphogenesis and cell division in Arabidopsis. *Journal of Cell Science* **120,** 4416–4425 (2007).
15. Furutani, I. *et al.* The SPIRAL genes are required for directional control of cell elongation in Aarabidopsis thaliana. *Development* **127,** 4443–4453 (2000).
16. Al-Bassam, J. *et al.* CLASP promotes microtubule rescue by recruiting tubulin dimers to the microtubule. *Dev Cell* **19,** 245–258 (2010).
17. Aumeier, C. *et al.* Self-repair promotes microtubule rescue. *Nat. Cell Biol.* **18,** 1054–1064 (2016).
18. Dogterom, M. & Leibler, S. Physical aspects of the growth and regulation of microtubule structures. *Physical Review Letters* **70,** 1347–1350 (1993).
19. Tindemans, S. H. & Mulder, B. M. Microtubule length distributions in the presence of protein-induced severing. *Phys Rev E Stat Nonlin Soft Matter Phys* **81,** 031910 (2010).
20. Wieczorek, M., Bechstedt, S., Chaaban, S. & Brouhard, G. J. Microtubule-associated proteins control the kinetics of microtubule nucleation. *Nat. Cell Biol.* **17,** 907–916 (2015).
21. Brouhard, G. J. & Rice, L. M. The contribution of αβ-tubulin curvature to microtubule dynamics. *The Journal of Cell Biology* **207,** 323–334 (2014).
22. Shaw, S. L., Kamyar, R. & Ehrhardt, D. W. Sustained microtubule treadmilling in Arabidopsis

cortical arrays. *Science* **300,** 1715–1718 (2003).
23. Sedbrook, J. C. MAPs in plant cells: delineating microtubule growth dynamics and organization. *Current Opinion in Plant Biology* **7,** 632–640 (2004).
24. Woody, S. T., Austin-Phillips, S., Amasino, R. M. & Krysan, P. J. The WiscDsLox T-DNA collection: an arabidopsis community resource generated by using an improved high-throughput T-DNA sequencing pipeline. *Journal of plant research* **120,** 157–165 (2007).
25. Alonso, J. M. *et al.* Genome-wide insertional mutagenesis of Arabidopsis thaliana. *Science* **301,** 653–657 (2003).
26. Klimyuk, V. I., Carroll, B. J., Thomas, C. M. & Jones, J. D. Alkali treatment for rapid preparation of plant material for reliable PCR analysis. *The Plant journal* **3,** 493–494 (1993).
27. Grefen, C. *et al.* A ubiquitin-10 promoter-based vector set for fluorescent protein tagging facilitates temporal stability and native protein distribution in transient and stable expression studies. *The Plant journal* **64,** 355–365 (2010).
28. Gutierrez, R., Lindeboom, J. J., Paredez, A. R., Emons, A. M. C. & Ehrhardt, D. W. Arabidopsis cortical microtubules position cellulose synthase delivery to the plasma membrane and interact with cellulose synthase trafficking compartments. *Nat. Cell Biol.* **11,** 797–806 (2009).
29. Clough, S. J. & Bent, A. F. Floral dip: a simplified method for Agrobacterium-mediated transformation of Arabidopsis thaliana. *The Plant journal* **16,** 735–743 (1998).
30. Paredez, A. R., Somerville, C. R. & Ehrhardt, D. W. Visualization of cellulose synthase demonstrates functional association with microtubules. *Science* **312,** 1491–1495 (2006).
31. Lindeboom, J. J. *et al.* Cortical Microtubule Arrays Are Initiated from a Nonrandom Prepattern Driven by Atypical Microtubule Initiation. *Plant physiology* **161,** 1189–1201 (2013).
32. Applegate, K. T. *et al.* plusTipTracker: Quantitative image analysis software for the measurement of microtubule dynamics. *Journal of structural biology* **176,** 168–184 (2011).
33. Thevenaz, P., Ruttimann, U. E. & Unser, M. A pyramid approach to subpixel registration based on intensity. *Ieee T Image Process* **7,** 27–41 (1998).
34. Papoulis, A. *Probability, random variables, and stochastic processes*. pp.103–104 (McGraw-Hill Companies, 1984).
35. Abramowitz, M. & Stegun, I. A. *Handbook of mathematical functions with formulas, graphs, and mathematical tables*. xiv–1046 p. (U.S. Govt. Print. Off., 1970).

Figures

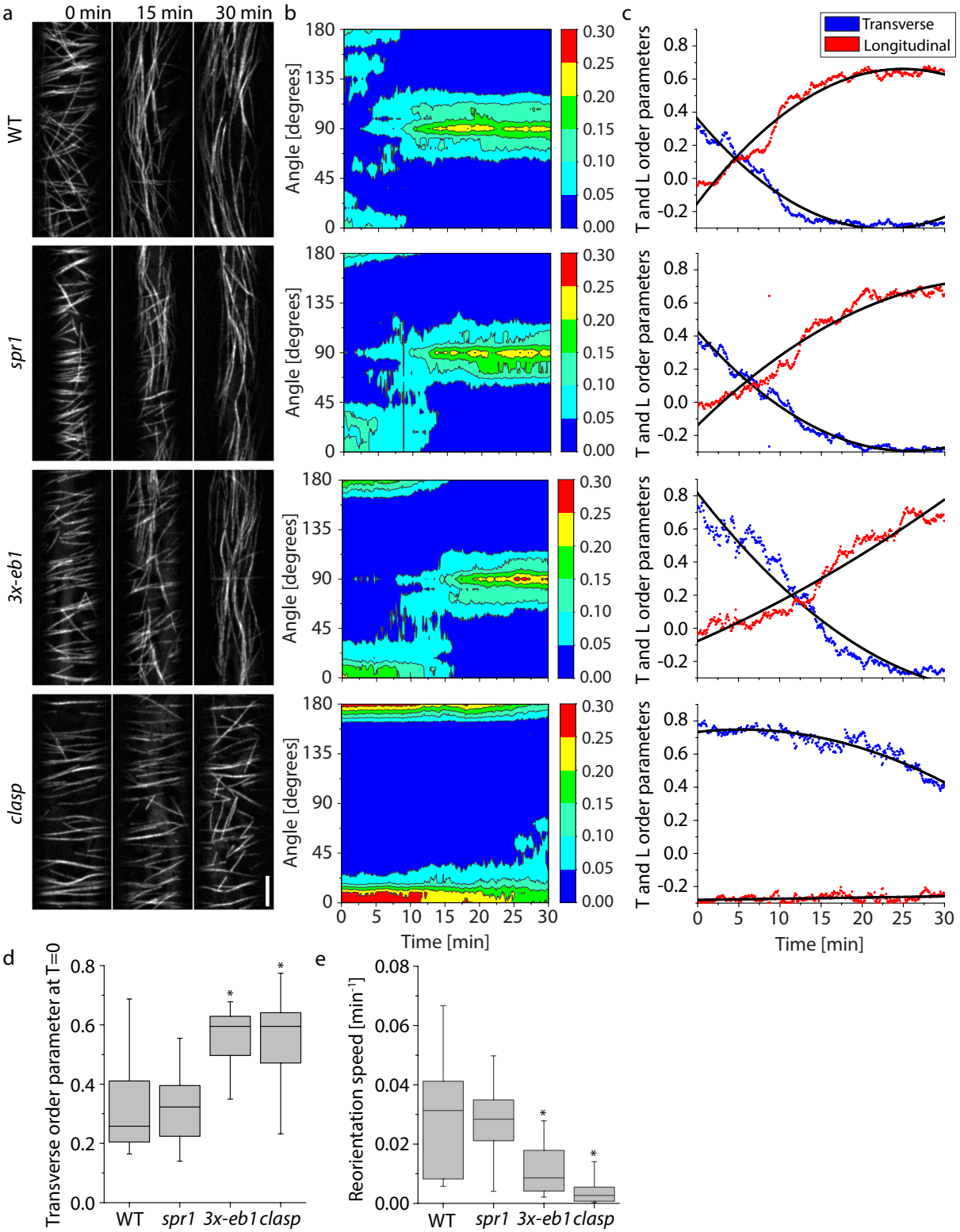

Figure 1 Microtubule reorientation in +TIP mutants. (a) Panels from confocal image time series of dark grown hypocotyl cells expressing YFP-TUA5 of WT, *spr1*, *3- eb1* and *clasp* mutant backgrounds at 0, 15 and 30 minutes. See Video 1. Scale bar is 5 µm. (b) Representative contour plots of MT orientation over time during blue light induced reorientation corresponding to the movies shown in (a). The color scale represents fraction of microtubules. (c) Longitudinal and Transverse

order parameters during blue light induced MT reorientation of the movies shown in (a). Black lines show quadratic fit. (d) Transverse order parameter at T = 0 of the cortical microtubules in the hypocotyl cells expressing YFP-TUA5 in WT (N = 8), *spr1* (N = 9), *3x-eb1* (N = 9) and *clasp* (N = 9). A Kruskal-Wallis test showed significant differences among the genotypes for the initial Transverse order parameter ($P < 0.01$). Asterisk represents significant difference form WT in Mann-Whitney U test ($P < 0.05$). (e) Longitudinal reorientation speed[2] of imaged microtubule arrays in etiolated hypocotyl cells expressing YFP-TUA5 in WT (N = 8), *spr1* (N = 9), *3x-eb1* (N = 9) and *clasp* (N = 9). A Kruskal-Wallis test showed significant differences for reorientation speed distributions among the genotypes ($P < 0.01$). Asterisk represents significant difference form WT in Mann-Whitney U test ($P < 0.05$). Boxplots show the 25th and 75th percentile as box edges, the line in the box indicates median value and the whiskers show the 2.5th and 97.5th percentile.

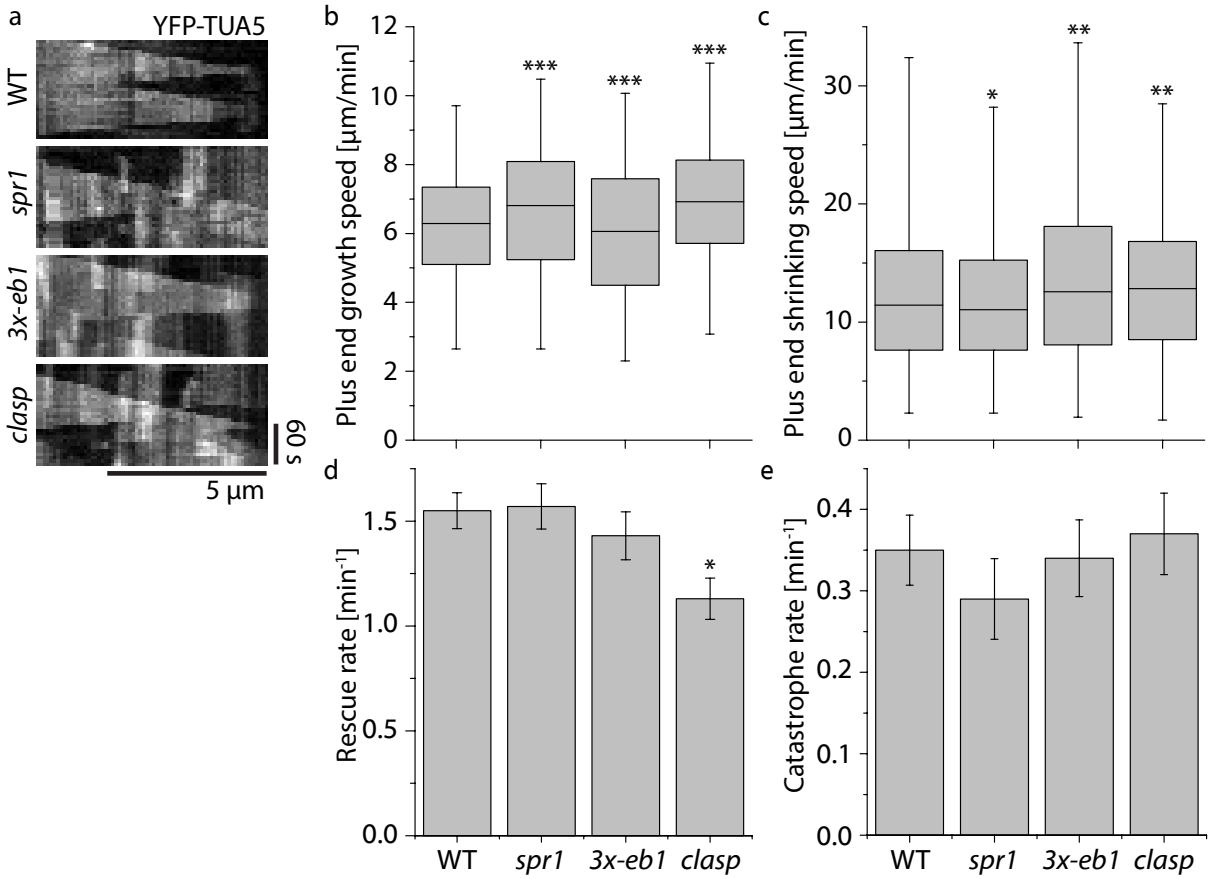

Figure 2 Microtubule plus end dynamics in +TIP mutants. (a) Kymographs of microtubules during early stages of blue light induced reorientation in WT, *spr1*, *3- eb1* and *clasp* mutant backgrounds expressing YFP-TUA5. (b) Boxplot of microtubule plus end growth speeds and (c) plus end shrinkage speeds in N = 2148, N = 1405, N = 1837, N = 1516 segments in 6 cells in WT, *spr1*, *3x-eb1* and *clasp* mutant backgrounds respectively. Asterisks indicate significant difference from WT. (d) Microtubule rescue rates (N = 213, N = 135, N = 110, N = 116 rescues in 6 cells, in WT, *spr1*, *3x-eb1* and *clasp* mutant backgrounds respectively). Error bars represent SEM. Asterisks indicate a significant difference by Rate Ratio test. (e) Microtubule rescue catastrophe rates (N = 190, N = 119, N = 155, N = 148 rescues in 6 cells, in WT, *spr1*, *3x-eb1* and *clasp* mutant backgrounds respectively). Error bars represent SEM. Asterisks indicate significant difference as compared to WT by Rate Ratio test. Significance depicted by * $P < 0.05$, ** $P < 0.01$ and *** $P < 0.001$.

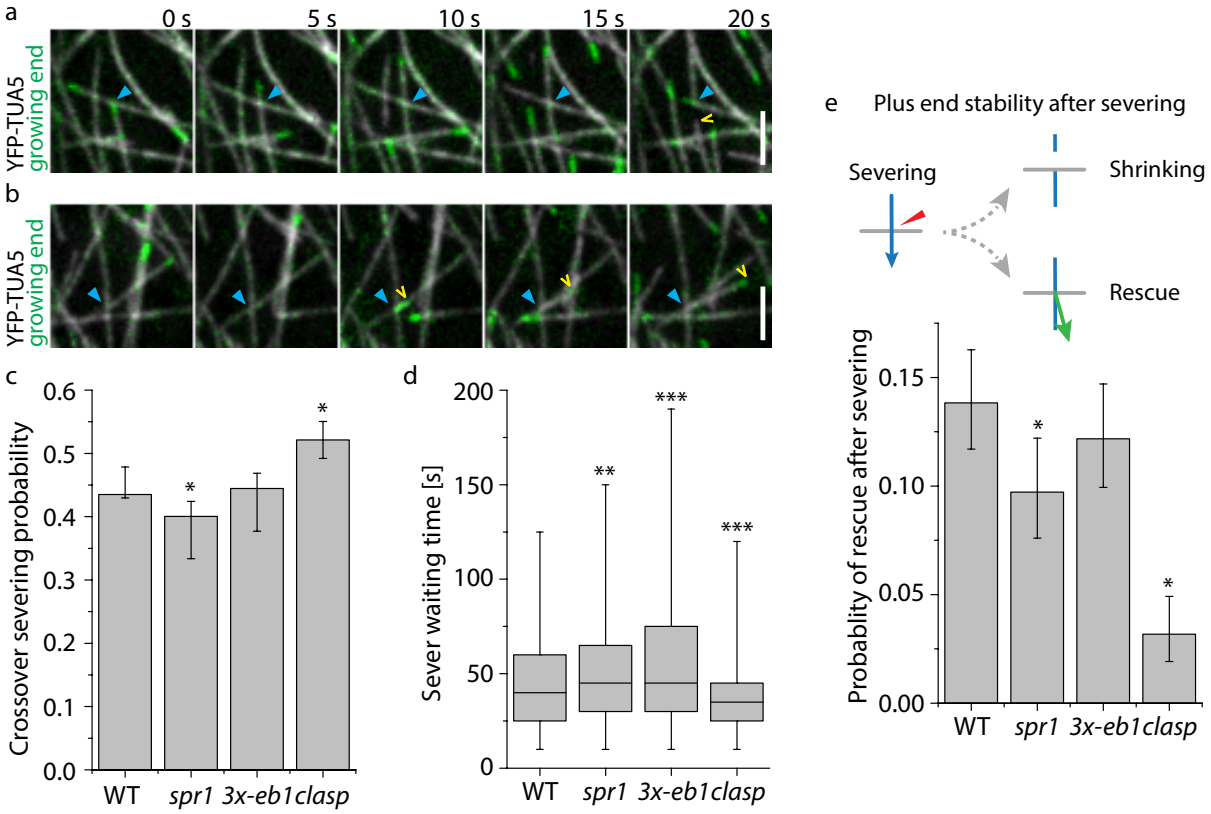

Figure 3 Microtubule crossover analysis in +TIP mutants. (a and b) Example of a crossover (blue arrowhead) where severing occurs, followed by (a) depolymerization (See Video 2) or (b) polymerization (See Video 3) of the new plus end (yellow arrowhead) in a WT cell expressing YFP-TUA5. Scale bars are 3 µm. (c) Severing probability per crossover in cells expressing YPF-TUA5 in WT, *spr1*, *3x-eb1,* and *clasp* backgrounds (N = 2027, 1696, 1718, and 1147 crossovers in 6 cells, respectively). Error bars show 95% confidence internals. Asterisks indicate a significant difference from WT by Fisher's exact test. (d) Waiting times from the observed moment of crossover generation until observed evidence for MT severing in WT, *spr1*, *3x-eb1,* and *clasp* backgrounds (N = 2027, 1696, 1718, and 1147 crossovers in 6 cells, respectively). Boxplots show the 25th and 75th percentile as box edges, the line in the box indicates median value and the whiskers show the 2.5th and 97.5th percentile. A Kruskal-Wallis test showed significant differences among reorientation speed distributions among the genotypes ($P < 0.001$). Asterisks indicate significant difference from WT by Mann-Whitney U test. (e) Probability of new plus ends created by severing at crossovers being initially observed in a growing state (N = 882, 679, 764, and 598 crossover severing events in WT, *spr1*, *3x-eb1,* and *clasp* backgrounds respectively). Error bars show 95% confidence intervals. Asterisks indicate a significant difference from WT by Fisher's exact test. Significance depicted by * $P < 0.05$, ** $P < 0.01$ and *** $P < 0.001$.

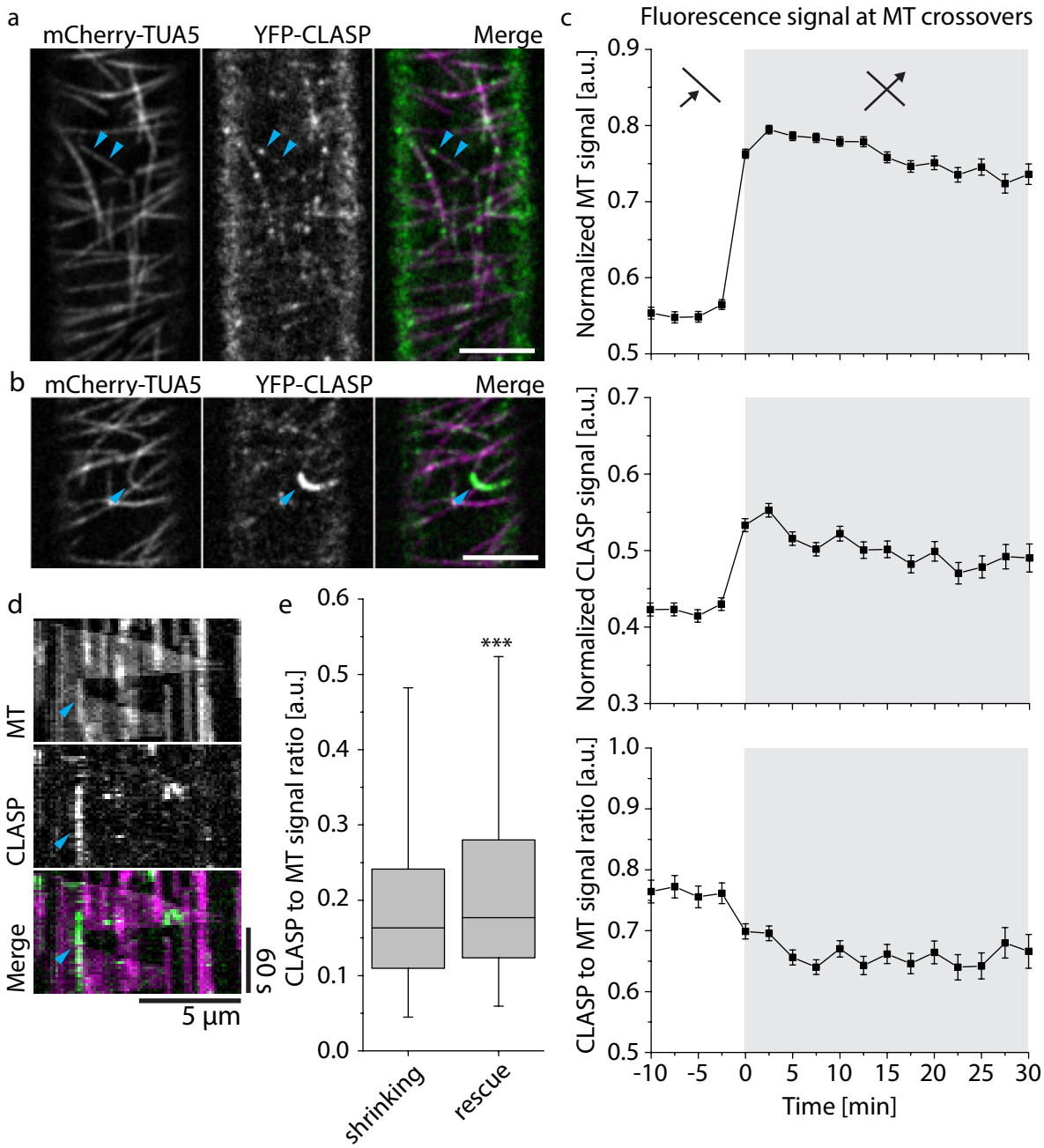

Figure 4 CLASP signal intensities at crossovers and rescue sites. (a) Example of MT and CLASP signal distribution in a 3-day old dark grown hypocotyl epidermal cell of a *clasp* mutant that is complemented by a YFP-CLASP construct and in addition expresses mCherry-TUA5. Cyan arrowheads show CLASP punctae along the microtubule lattice. See Video 4. Scale bar 5 µm. (b) MT and CLASP signal intensities during crossover formation. The top panel shows the relative MT signal intensity, the middle panel the relative CLASP signal intensity and the bottom panel shows the ratio of CLASP to MT signal intensity (N = 839 crossovers in 6 plants). The white background indicates the time before the crossovers are formed and the gray background indicates the time at which the crossover is formed. (c) Kymograph of a MT rescue event coinciding with high CLASP signal intensity. Cyan arrowhead indicates the point of MT rescue. (d) Boxplot of CLASP to MT signal intensity ratio for microtubules that continue shrinking and microtubules that get rescued. Boxplots

show the 25th and 75th percentile as box edges, the line in the box indicates median value and the whiskers show the 2.5th and 97.5th percentile. Microtubules were observed shrinking in 2716 frames and we observed rescue 301 times. CLASP to MT signal intensity ratios were shown to be significantly higher in locations where the rescues occurred by Mann-Whitney U test. Significance depicted by * $P < 0.05$, ** $P < 0.01$ and *** $P < 0.001$. (e) Example of high CLASP signal intensity on highly curved microtubule in 3-day old dark grown hypocotyl epidermal cell expressing YFP-CLASP and mCherry-TUA5. See Video 4. Scale bar 5 µm.

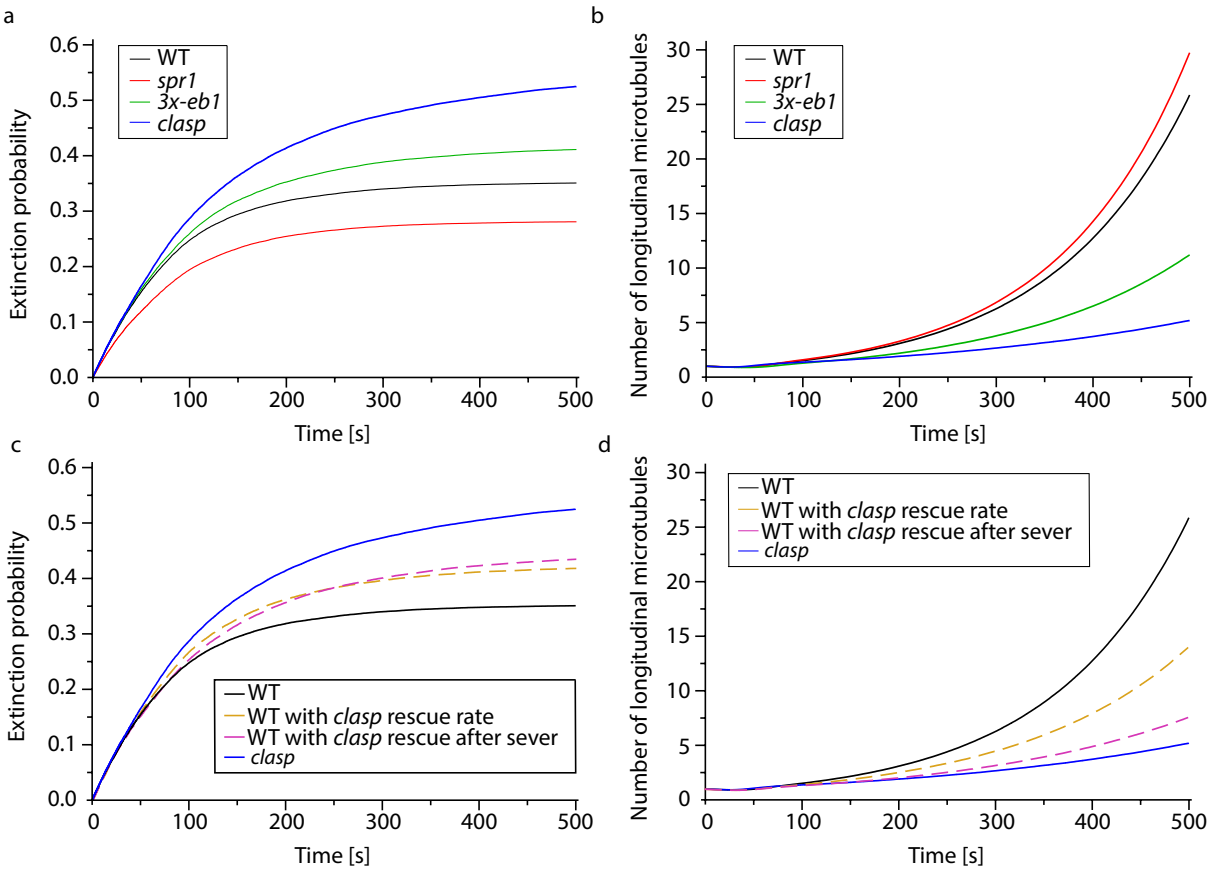

Figure 5 Simulation of microtubule amplification driven by severing. (a) Time evolution of the fraction of extinctions in WT, *spr1*, *3x-eb1*, and *clasp* mutants. Extinctions are more likely in less stable mutants, i.e. in mutants that are less deep into the unbounded growth regime. (b) Time evolution of the average number of microtubules during the amplification process shows that a lower probability of rescue after severing and a less deep unbounded growth regime in *3x-eb1* and *clasp* mutants result in a slower amplification as compared to *spr1* and WT. (c) Time evolution of the fraction of extinctions in WT with *clasp* intrinsic rescue rate, and WT with *clasp* rescue after severing probability *in silico* mutants, shows that even if the two reduced rescue parameters have a similar effect on the extinction probability, (d) the probability of rescue after severing $P_{s,+}$ has a greater impact on the amplification process. Indeed WT microtubules with *clasp* $P_{s,+}$ perform an amplification that almost completely reproduces the *clasp* results (dashed purple curve).

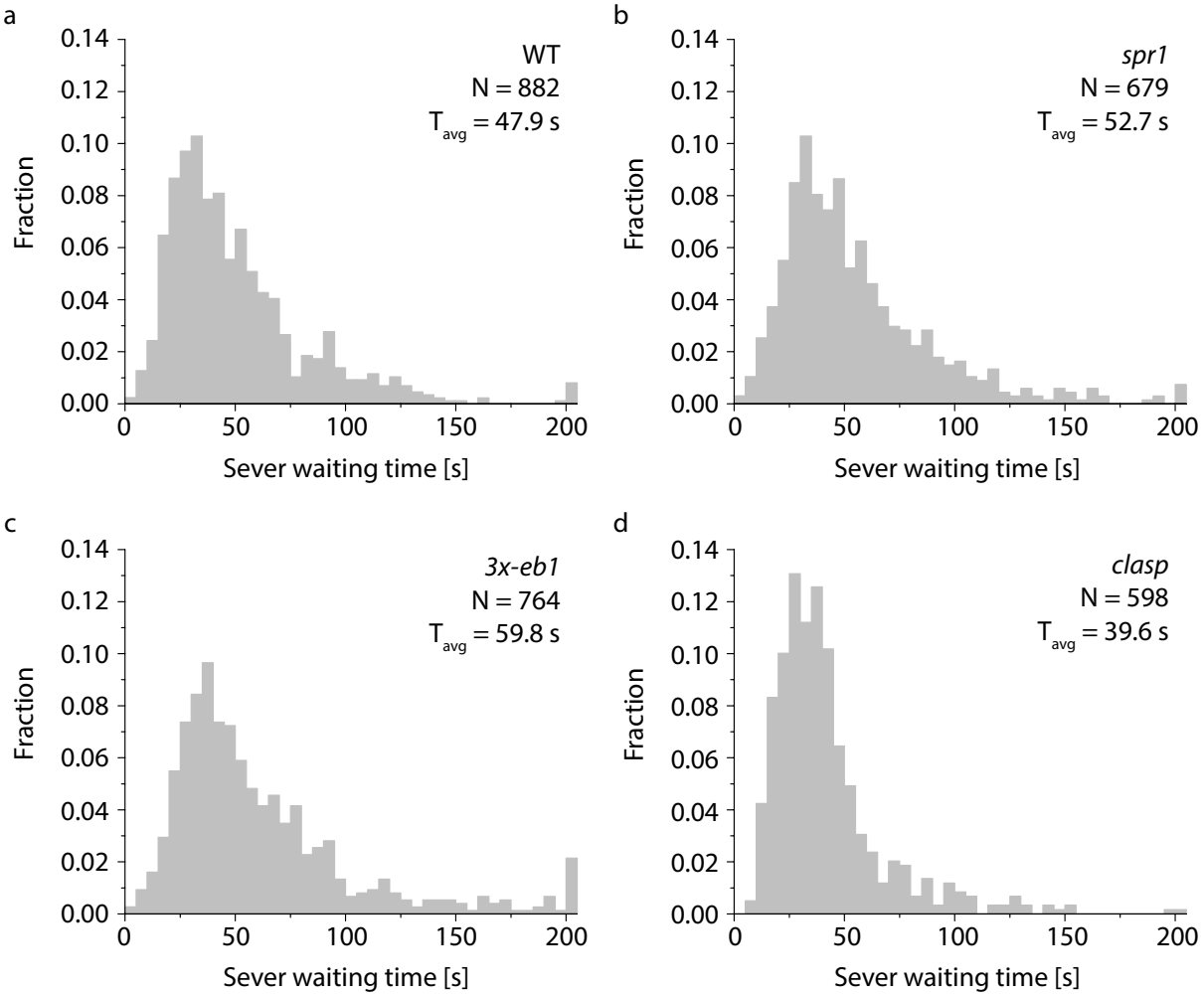

Figure S1 Sever waiting time distributions and severing preferences. (a-d) Distribution of sever waiting times from the moment the crossover is formed in (a) WT, (b) *spr1*, (c) *3x-eb1* and (d) *clasp*. Six plants were used for each genotype. Sever waiting times > 200 s are added up and shown in the last bin.

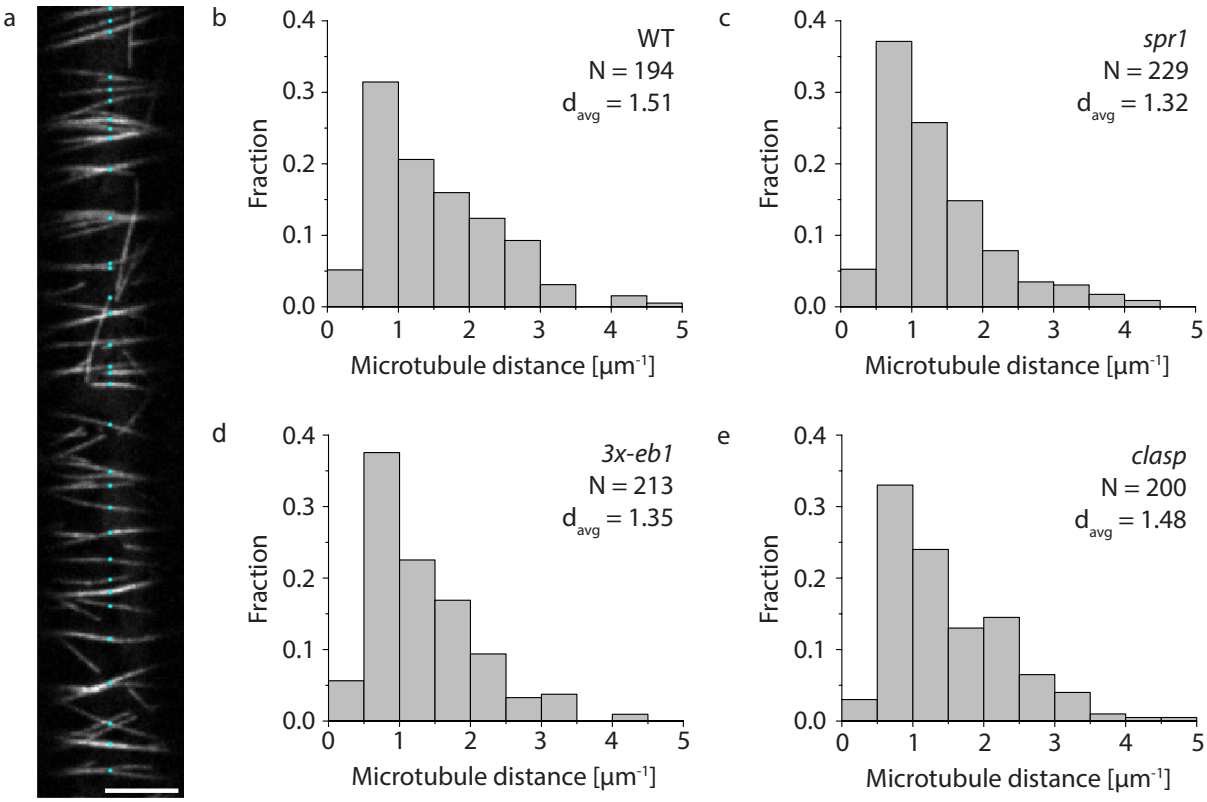

Figure S2 Longitudinal microtubule distances. (a) WT example image with detected microtubules labeled in cyan. Scale bar 5 µm. (b-e) Histogram of microtubule distances in (b) WT, (c) *spr1*, (d) *3x-eb1* and (e) *clasp*. Number of detected microtubules indicated by N, d_{avg} is the average distance between microtubules in µm, we used 6 cells per genotype. A Kruskal-Wallis test followed by a Mann-Whitney U test shows that the distribution of bundle distances only differs significantly from WT for *spr1* ($P < 0.05$).

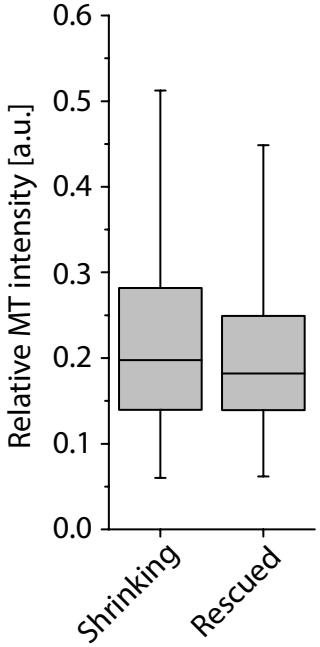

Figure S3 Microtubule signal does not positively correlate with rescue events. Boxplot of relative MT signal intensity on microtubules that continue shrinking and microtubules that get rescued. Boxplots show the 25th and 75th percentile as box edges, the line in the box indicates median value and the whiskers show the 2.5th and 97.5th percentile. Microtubules were observed shrinking in 2716 frames and we observed rescue 301 times. The relative MT signal was not significantly higher for instances of microtubule rescue ($p > 0.98$ Mann-Whitney U test).

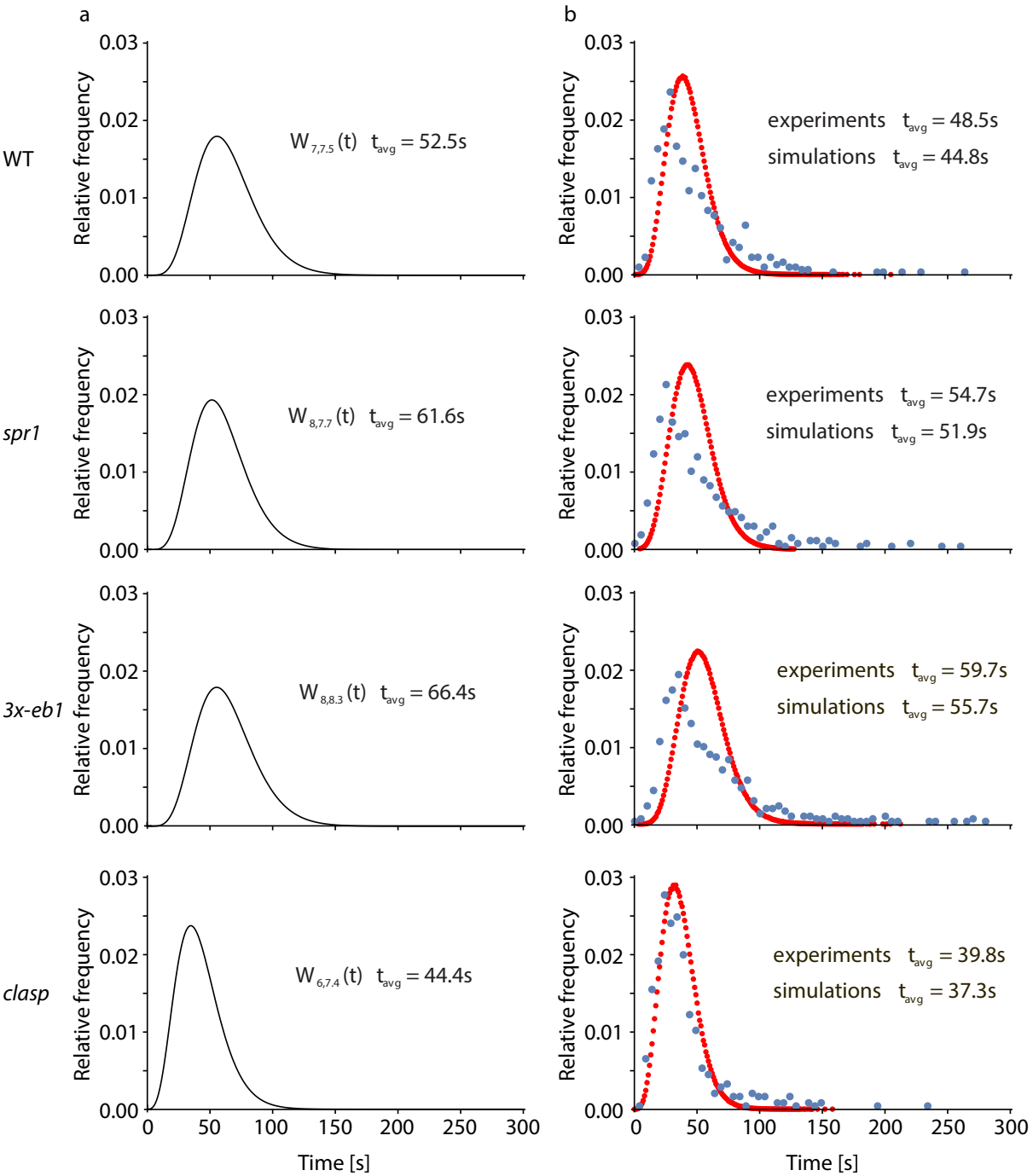

Figure S4 The optimal intrinsic severing waiting time distribution used in simulations (a), and the comparison between computed conditional severing waiting time distribution (red dots) and experimentally measured distribution (blue dots), for WT, *spr1*, *3x-eb1*, and *clasp* (b).

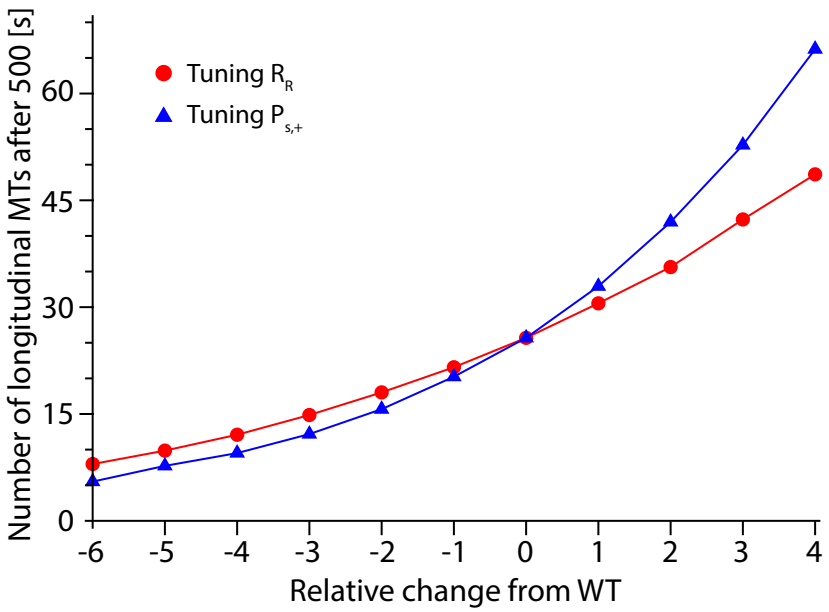

Figure S5 Number of longitudinal microtubules in the simulations after 500s as $P_{s,+}$ and r_r are varied. Blue triangles represent WT microtubules with changed rescue after severing probability, respectively $P_{s,+} = 0$, $P_{s,+} = 0.025$, $P_{s,+} = 0.05$, $P_{s,+} = 0.075$, $P_{s,+} = 0.1$, $P_{s,+} = 0.125$, $P_{s,+} = 0.15$, $P_{s,+} = 0.175$, $P_{s,+} = 0.2$, $P_{s,+} = 0.225$, and $P_{s,+} = 0.25$. Red dots represent WT microtubules with changed intrinsic rescue rate, respectively r_r = 0.76 events/min, r_r = 0.89 events/min, r_r = 1.03 events/min, r_r = 1.16 events/min, r_r = 1.30 events/min, r_r = 1.43 events/min, r_r = 1.56 events/min, r_r = 1.69 events/min, r_r = 1.83 events/min, r_r = 1.96 events/min, and r_r = 2.09 events/min.

Table S1: Simulation parameters

Parameter	Description	WT	*spr1*	*3x-eb1*	*clasp*	Units
v^+	plus end growth velocity	6.2	6.6	6.1	7.0	μm min^{-1}
v^-	plus end shrinking velocity	13.5	12.4	14.9	13.5	μm min^{-1}
r_r	rescue rate	1.56	1.57	1.42	1.12	min^{-1}
r_c	catastrophe rate	0.35	0.29	0.34	0.37	min^{-1}
d_{avg}	average microtubule spacing distance	1.51	1.32	1.35	1.48	μm
$P_{s,+}$	probability of rescue after severing	0.15	0.10	0.13	0.03	-
k	shape parameters of gamma distribution	7	8	8	6	-
θ	scale parameters of gamma distribution	7.5	7.7	8.3	7.4	s
D	mean microtubule spacing	1.01	0.82	0.85	0.98	μm

Supplemental Table S2. Primers used to score by PCR the presence or absence of corresponding T-DNA insertions in *Ateb1a-2* (WiscDsLox481-484J12), *Ateb1b-2* (WiscDsLox331A08), and *Ateb1c-2* (SALK_018475) segregants.

Primer	**Sequence**	**PCR product size (detecting)**
AtEB1a_F2	AGCAGCTGAAGTGCAGGCTTTGTC	F2+R1= 360 bp (*AtEB1a* Wild Type)
AtEB1a_R1	TGGAAAACTTGTCTTGGAGCTAAATAGTG	F2+P745= ~300 bp (*Ateb1a-2* T-DNA)
WiscDSLOX_P745	AACGTCCGCAATGTGTTATTAAGTTGTC	
AtEB1b_F3	GACCACTAGACAATTTGGAGTTTCTTCAA	F3+R3= 674 bp (*AtEB1b* Wild Type)
AtEB1b_R3	CGGAAGATCATCGAGTTCAGGAGTCTG	F3+P745= ~600 bp (*Ateb1b-2* T-DNA)
AtEB1c_F1	CGGATTTGGAATTGGATCTTACGATTATC	
AtEB1c_R1	GAACAAACTTACTTATGCTGGCCTCCATT	F1+R1= 557 bp (*AtEB1c* Wild Type)
LBb1	GCGTGGACCGCTTGCTGCAACT	F1+LBb1= ~610 bp (*Ateb1c-2* T-DNA)

Primer WiscDSLOX_P745 and LBb1 anneal to the respective left-border T-DNA sequences whereas the other primers anneal to genomic sequences flanking each T-DNA.

Supplementary movie legends

Video 1: Blue light induced microtubule reorientation in dark grown hypocotyl epidermal cells expressing YFP-TUA5 in WT, *spr1*, *3x-eb1* and *clasp* genetic backgrounds.

Video 2: Example of crossover severing event in a WT dark grown hypocotyl epidermal cell that generates a shrinking new plus end. The cyan arrowhead marks the microtubule crossover site. The yellow '>' marks the new plus end. Growing microtubule ends are shown in green.

Video 3: Example of crossover severing event in a WT dark grown hypocotyl epidermal cell that generates a growing new plus end. The cyan arrowhead marks the microtubule crossover site. The yellow '>' marks the new plus end. Growing microtubule ends are shown in green.

Video 4: Time lapse movie of CLASP and MT colocalization in dark grown hypocotyl epidermal cell in a *clasp* mutant rescued with a YFP-CLASP construct and co-expressing mCherry-TUA5.

Video 5: Example time lapse Video showing strong CLASP label on highly curved microtubules. Highly curved microtubules are marked by a cyan arrowhead. The example movie features a dark grown epidermal hypocotyl cell of a *clasp* mutant rescued with a YFP-CLASP construct and co-expressing mCherry-TUA5.

Video 6: Example of a section of a WT cell expressing YFP-TUA5 dark grown hypocotyl cell where all the identified crossovers are marked with a yellow '+'-sign. Growing microtubule ends are shown in green.